Effect of the Total Angular Momentum on the Dynamics of the $H_2 + H_2$ System†

Ernesto Garcia,*,‡ Amaia Saracibar,‡ Carlos Sánchez,‡ and Antonio Laganà*,§

Departamento de Quimica Fisica, Universidad del Pais Vasco, 01006 Vitoria, Spain, and Dipartimento di Chimica, Università di Perugia, 06123 Perugia, Italy

Received: April 3, 2009; Revised Manuscript Received: May 18, 2009

Extended full-dimensional quasiclassical trajectory calculations have been performed for the H_aH_b ($v_{ab} = 10$, 11, 12, 13, 14, $j_{ab} = 0$) + H_cH_d ($v_{cd} = 0$, $j_{cd} = 0$) collisions at values of the translational energy ranging from threshold to 1.5 eV and values of the total angular momentum quantum number J varying from zero to very large ones. Collision-induced dissociation, four-center exchange reaction, and single exchange process probabilities have been calculated. Full-dimensional classical calculations were found to reproduce well the corresponding ($J = 0$) quantum results, including the thresholds. In contrast, the agreement of full-dimensional classical calculations with the corresponding both quantum and classical reduced dimensionality ones was found to be poor. The effect of varying J on the efficiency of the various processes has also been investigated. Four-center reactions were found to be favored by low values of J, whereas dissociation processes were found to be favored by higher values of J, as expected from the fact that energy exchange takes place at longer range than mass exchange. To evaluate to what extent the $J = 0$ full-dimensional calculations represent the unconstrained dynamics of the system, J-shift model classical results were compared with the all-J ones. Product vibrational distributions for both partially dissociative and exchange processes were also found to depend significantly on the value of J.

Introduction

Detailed information on the kinetics and the dynamics of the four-atom $H_2 + H_2$ system is of key importance in modeling several gas phase nonequilibrium complex technological processes, such as combustion,[1,2] spacecraft re-entry,[3−5] and negative ion production from plasmas.[6,7] Collisional energy transfer in the $H_2 + H_2$ system is also important in some natural processes, such as those occurring when shock waves cross the interstellar molecular clouds.[8−10] In particular, for example, hydrogen molecules may increase their vibrational excitation and, via collision and ladder-climbing mechanisms, even dissociate.[11,12] This prompted a great deal of theoretical work aimed at building an accurate potential energy surface (PES) and at carrying out detailed dynamics and kinetics investigations.

Recently, some accurate investigations of the PES of the $H_2 + H_2$ system were reported in the literature. All these PESs were based on high level ab initio calculations' extending to four atoms the multireference method and basis set already adopted by Siegbhan and Liu in their calculations for the $H + H_2$ system.[13] In this way, the potential energy values of the $H_2 + H_2$ system were computed for an extended set of molecular geometries (48 180).[14,15] The first global accurate functional representation of the $H_2 + H_2$ PES was published by Aguado et al. (ASP)[16] who interpolated the ab initio values using a many-body expansion based on a modified version of the bond order coordinates.[17,18] On the ASP PES, the geometry of H_4 at the saddle point is collinear, and the distance between the two external hydrogen atoms is 1.697 Å, whereas that between the two internal atoms is 0.748 Å (i.e., slightly larger than the equilibrium distance of the isolated hydrogen molecule, 0.741 Å). The energy at the saddle (4.82 eV) is larger than the dissociation energy of the isolated hydrogen molecule (4.75 eV) and the energy of the H_aH_b ($v_{ab} = 11$, $j_{ab} = 0$) + H_cH_d ($v_{cd} = 0$, $j_{cd} = 0$) asymptote (with v and j being the vibrational and rotational quantum states of the diatom, respectively). Moreover, the dissociation of one hydrogen molecule as a result of a collision with another hydrogen molecule, leading to a product molecule in its ground vibrotational state, needs an energy of at least 5.02 eV. This value is about 0.2 eV larger than that of the saddle and, therefore, allows dissociation and exchange processes to coexist. Later on, a new PES (BKMP) was published.[15] The BKMP PES makes use for the interpolation of a hybrid functional form made of the ASP function and the extended $H + H_2$ functional proposed by Truhlar and Horowitz.[19]

As already mentioned, collisions between two hydrogen molecules can lead to several kinds of processes. In fact, in addition to the inelastic processes and the full-dissociation ones, exchange (1) and partial dissociation, either nonreactive (2) or reactive (3), can take place:

$$\text{(4C)}\quad H_aH_b + H_cH_d \rightarrow H_aH_d + H_bH_c,\ H_aH_c + H_bH_d \tag{1}$$

$$\text{(CID)}\quad H_aH_b + H_cH_d \rightarrow H_a + H_b + H_cH_d,\ H_aH_b + H_c + H_d \tag{2}$$

$$\text{(SE)}\quad H_aH_b + H_cH_d \rightarrow H_aH_c + H_b + H_d,\ H_aH_d + H_b + H_c,\ H_bH_c + H_a + H_d,\ H_bH_d + H_a + H_c \tag{3}$$

Processes of type 1 are four-center (4C) reactions. 4C processes are a typical feature of reactions of systems having

† Part of the "Vincenzo Aquilanti Festschrift".

* Corresponding author. E-mail: e.garcia@ehu.es; lag@dyn.unipg.it.
‡ Universidad del Pais Vasco.
§ Università di Perugia.

10.1021/jp903072j
Published on Web 06/17/2009

more than three atoms, since two bonds are broken and formed at the same time. Processes of type 2 (CID) are collision-induced dissociations or nonreactive dissociations in which only one of the two initial bonds is broken. Processes of type 3 (SE) are single exchange processes or reactive dissociations in which both the two initial bonds are broken but only one new bond is formed.

The coexistence of several processes, including the dissociative ones, the high energy required to surmount the barrier, and the six degrees of freedom involved in a full dynamical treatment are a truly insurmountable obstacle to the carrying out of exact quantum studies of the exchange and dissociation above-mentioned $H_2 + H_2$ processes. In the past, this has prompted the use of quantum (QM) reduced dimensionality and quasiclassical (QCT) (full-dimensional and reduced dimensional) techniques. A first QM time-independent calculation performed using a reduced dimensionality (3 degrees of freedom) approach considering one highly vibrationally excited molecule and the other one in the ground vibrational state was carried out by Hernández and Clary.[20] In the model, the atoms were assumed to occupy the four corners of a plane trapezoid, and the degrees of freedom considered for the time-independent quantum dynamical investigation were the ones associated with the relative translation of the two vibrating molecules, excluding any kind of rotation. The same model was subsequently used by Hernández, Campos et al. for a QM time-dependent study of the title reaction[21] and isotopic substitutions.[22] The same group carried out another QM time-dependent reduced dimensionality study by varying the collision geometries (H-, X-, T-, and L-shaped geometries were used) with one molecule being highly vibrationally excited (and the other in the ground vibrational state).[23] More recently also, a comparison with the analogous reduced dimensionality QCT studies were reported.[24]

Full-dimensional QCT computational studies of the dynamics of the $H_2 + H_2$ system were started long before the quantum ones[25−28] and led to the development of a dynamical model for four-center reactions.[29−31] The most recent of them were carried out by our group on the ASP PES. In particular, our group studied the dynamics and the kinetics of $H_2 + H_2$ using both the full dimensionality and the reduced dimensionality trapezoidal model to compare with quantum results.[32,33] The mechanisms of the exchange and of the dissociation processes were investigated also for the isotopic variants $H_2 + HD$ and $H_2 + D_2$.[34] Finally, state-to-state rate coefficients for the CID, 4C, and SE processes for several combinations of initial vibrational states at temperatures of 1000, 2000, and 4000 K were also computed.[35] Mandy et al. studied the effect of the translational, rotational and vibrational energy on dissociation using full-dimensional quasiclassical trajectories,[12,36] and for some particular geometries (H, X, and T), they made a comparison with QM results.[37] Another burst of interest in the study of the collision between two hydrogen molecules has led to the calculation of nonreactive vibrotational de-excitation cross sections using full-dimensional quantum methods of both time-independent[38−42] and -dependent[43−47] type.

However, the most important step forward in the accurate calculation of the probabilities of the CID, 4C, and SE processes for the H_aH_b ($v_{ab} = 10, 11, j_{ab} = 0$) + H_cH_d ($v_{cd} = 0, j_{cd} = 0$) collisions was represented by the work reported in ref 48, in which full-dimensional QM time-dependent results are discussed. The calculations were carried out at zero total angular momentum quantum number ($J = 0$) for state-specific probabilities and were used also to check the validity of previous reduced dimensionality calculations.[49]

In this work, we report full-dimensional QCT calculations mimicking the energetic conditions of the quantum calculations of ref 48 and extending the investigation to nonzero values of J. The aim of such calculations is two-fold: The first is to carry out an extended check of the validity of classical versus quantum approaches for the $H_2 + H_2$ system. The second is to study the effect of the total angular momentum on (a) the energy dependence of the probability of the different processes in which the $H_2 + H_2$ collision can branch and (b) the way energy is disposed to the products. Accordingly, the paper is organized as follows: in the second section, the calculations performed and the properties evaluated are illustrated; in the third section, the computed $J = 0$ quasiclassical probabilities are analyzed; in the fourth section, similarities and differences between quasiclassical and quantum probabilities are investigated. Finally, the effect of increasing J on quasiclassical probabilities (and therefore, the validity of the J-shift approximations) and on product internal energy is discussed in the fifth and sixth sections, respectively.

Computational Details and Outcomes

In this work, the quasiclassical trajectory VENUS program[50] and the ASP PES (the same adopted by the QM calculations of ref 48) were used. Accordingly, a first set of calculations was carried out at $J = 0$ to carry out a detailed comparison of QCT and QM probabilities. The second set of calculations was carried out at increasing values of the total angular momentum quantum number ($J > 0$) so as to evaluate the effect of higher total angular momentum collisions in CID, 4C, and SE processes.

The initial conditions for the collisions mimicked those of ref 48. In particular, the vibrational states of the initial molecules were set to $v_{ab} = 9$, 10, 11, 12, 13, and 14 for one of them (four states more than in ref 48) and $v_{cd} = 0$ for the other. The initial rotational states for both molecules were set to be the ground state, $j_{ab} = j_{cd} = 0$.

In this work, translational energies (E_{tr}) considered for the $J = 0$ calculations were increased from 0.1 to 1.5 eV in steps of 0.1. However, to gain accuracy at threshold, calculations were performed by varying the energy in steps of 0.02 eV. In the case of $J > 0$, translational energies considered for the calculations were $E_{tr} = 0.6$, 0.8, 1.0, 1.2, and 1.4 eV.

The orientation of the initial molecules in the space and the vibrational phases were selected randomly. An integration step of 0.15 fs was used to guarantee a good total energy and angular momentum conservation. The integration was stopped when at least four of the six diatomic distances exceeded 8.0 Å, then the nature of the process was determined, and the vibrational and rotational quantum numbers were assigned to the bound diatoms. In this work, no restrictions for the zero point energy were enforced into the results.

Calculated quantities were partial (fixed J) probabilities, P^J; partial cross sections, σ^J; and product vibrational distributions (PVDs) for the CID, 4C, and SE processes (for the sake of simplicity, labels of the internal energy states are not explicitly quoted). For the various processes, fixed J probabilities were calculated as

$$P^{J,\mathrm{CID}} = \frac{N^{J,\mathrm{CID}}}{N^J} \qquad P^{J,4\mathrm{C}} = \frac{N^{J,4\mathrm{C}}}{N^J} \qquad P^{J,\mathrm{SE}} = \frac{N^{J,\mathrm{SE}}}{N^J} \tag{4}$$

where $N^{J,\mathrm{CID}}$, $N^{J,4\mathrm{C}}$, and $N^{J,\mathrm{SE}}$ are the number of trajectories leading to, respectively, the CID, 4C, and SE processes out of

the total number N^J of integrated trajectories at a given value of J. Fixed J cross sections were calculated using the definition of Aoiz et al.[51] as

$$\sigma^{J,\mathrm{CID}} = \frac{\pi\hbar^2}{2\mu E_{\mathrm{tr}}}(2J+1)P^{J,\mathrm{CID}}$$
$$\sigma^{J,\mathrm{4C}} = \frac{\pi\hbar^2}{2\mu E_{\mathrm{tr}}}(2J+1)P^{J,\mathrm{4C}}$$
$$\sigma^{J,\mathrm{SE}} = \frac{\pi\hbar^2}{2\mu E_{\mathrm{tr}}}(2J+1)P^{J,\mathrm{SE}} \quad (5)$$

where μ indicates the reduced mass of the reactant system. By summing the fixed J cross sections over the total angular momentum quantum number, one obtains the integral cross sections[51]

$$\sigma^{\mathrm{CID}} = \sum_{J=0}^{J_{\max}} \sigma^{J,\mathrm{CID}}$$
$$\sigma^{\mathrm{4C}} = \sum_{J=0}^{J_{\max}} \sigma^{J,\mathrm{4C}}$$
$$\sigma^{\mathrm{SE}} = \sum_{J=0}^{J_{\max}} \sigma^{J,\mathrm{SE}} \quad (6)$$

where $J_{\max}$ represents the maximum value of J with a nonzero probability for the given process. Fixed J PVDs were calculated as follows:

$$P_{v'}^{J,\mathrm{CID}} = \frac{N_{v'}^{J,\mathrm{CID}}}{N^J} \qquad P_{v'}^{J,\mathrm{4C}} = \frac{N_{v'}^{J,\mathrm{4C}}}{N^J} \qquad P_{v'}^{J,\mathrm{SE}} = \frac{N_{v'}^{J,\mathrm{SE}}}{N^J} \quad (7)$$

where $N_{v'}^{J,\mathrm{CID}}$, $N_{v'}^{J,\mathrm{4C}}$, and $N_{v'}^{J,\mathrm{SE}}$ are the number of trajectories ending with a product vibrational energy assignable to the v' vibrational state for the CID, 4C, and SE processes, respectively.

Batches of at least 500 000 trajectories were integrated for each set of initial conditions, totalling about one-half billion trajectories. The corresponding huge computational effort was kindly provided by the Spanish Supercomputing Network[52] and the segment of the production Grid of EGEE[53] available to the COMPCHEM virtual organization.[54,55] Thanks to the large number of integrated trajectories, the error bar associated with the calculated probabilities and cross sections is smaller than 2% (with the exception of those just about the threshold).

$J = 0$ Quasiclassical Probabilities

To start our analysis, we examine first, in detail, QCT results and compare the efficiency of various processes at different initial conditions (state-specific). As already mentioned, our study covers an interval of reactant vibrational states larger than that of the quantum study of ref 48. The state-specific (the mention to state specificity will be dropped hereafter when not strictly necessary) probabilities calculated for the H_aH_b (v_{ab} = 9, 10, 11, 12, 13, 14, $j_{ab} = 0$) + H_cH_d ($v_{cd} = 0$, $j_{cd} = 0$) CID (upper panels), 4C (central panels), and SE (lower panels) processes are plotted in Figure 1 as a function of both the collision (left-hand panels) and the total (right-hand panels) energy. As apparent from the Figure, the CID (the nonreactive dissociative process; that is, the dissociation of the vibrationally excited hydrogen molecule) is the dominant process at low collision energy (for example, at $v_{ab} = 14$, its probability amounts to 0.8). Yet, as the collision energy increases, the probability of 4C (the four-center exchange process) increases to the point of competing with CID (its value is 0.4 at $E_{tr} = 1.5$ eV and $v_{ab} = 13$ or 14). The probability of SE (the reactive dissociative process) is always significantly lower than that of the other processes and only for $v_{ab} = 14$ at high collision energy does it increase up to 0.1.

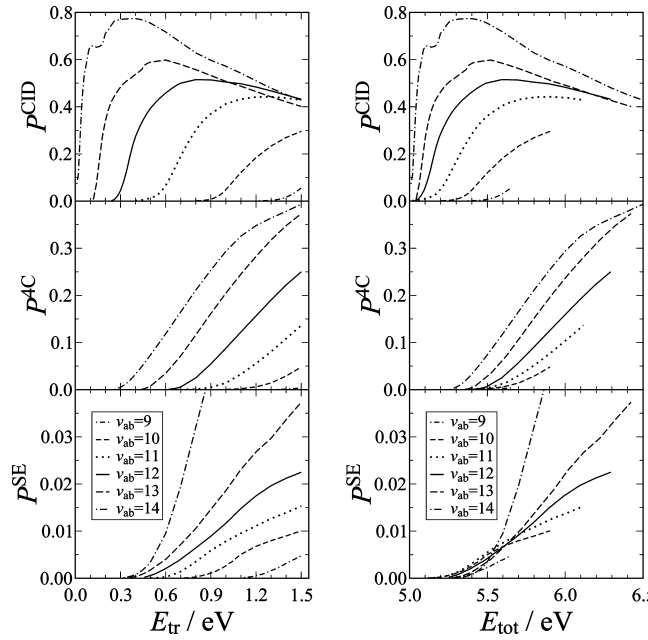

Figure 1. QCT CID (upper panels), 4C (central panels), and SE (lower panels) probabilities calculated at $J = 0$ for H_aH_b (v_{ab} = 9, 10, 11, 12, 13, 14, $j_{ab} = 0$) + H_cH_d ($v_{cd} = 0$, $j_{cd} = 0$), plotted as a function of collision energy (left-hand panels) and total energy (right-hand panels).

Figure 1 shows also that for all the processes considered, the probability curves exhibit the typical behavior of collisions having a barrier to reaction. This means that they show an appreciable energy threshold and a following increasing trend with energy that is easily modeled using a hard sphere treatment. Still, however, some important differences can be singled out when comparing the detail of the probability curves for different types of processes and vibrational states.

For example, when comparing the CID probabilities, plotted in the upper panels of Figure 1 as a function of the translational energy (left-hand panel) and as a function of the total energy (right-hand panel), it becomes apparent that the threshold of CID processes depends on the vibrational excitation. Accordingly, at low vibrational excitation of the reactants (v_{ab} = 9, 10), additional energy needs to be supplied as collisional to enable the system to reach the dissociation limit (5.02 eV), whereas this is not needed when vibrational excitation is high (v_{ab} = 11−14). Moreover, the increase in the probability with collision energy is sharp for $v_{ab} = 14$ and quite smooth for v_{ab} = 11. These results also show that vibrational energy is more efficient than translational energy in promoting nonreactive dissociation for all the vibrational states considered here (and not only for the v_{ab} = 10, 11 states considered in ref 48).

For $v_{ab} = 14$, the CID probability exhibits a small structure at E_{tr} = 0.1−0.3 eV, which also appears in both reduced dimensionality quantum[21] and classical[34] results. This structure is the fingerprint of the competition of two microscopic

mechanisms in which the hydrogen molecule in the ground vibrational state either passes through the other molecule or bounces back. This rebound-like mechanism was found to be dominant at low collision energy and to be the one giving rise to the maximum occurring at $E_{tr} = 0.1$ eV. In contrast, the insertion mechanism was found to prevail when the collision energy increases, generating the maximum at $E_{tr} = 0.3$ eV. At larger collision energies, the two mechanisms were found to contribute comparably.

The central panels of Figure 1 show the probability calculated for the 4C four-center exchange reactions. 4C results also, as the already found for the CID ones, bear the typical behavior characterizing the collisions overtaking an energetic barrier and are easily understandable in terms of a hard sphere treatment. There are, however, some important differences to emphasize. The thresholds of the 4C processes are significantly higher than those of the CID ones because of the more severe dynamical constraints applying to the former. These constraints also make the $v_{ab} = 14$ probability increase more mildly with energy and lack of the structure associated with the competition between insertion and rebounding mechanisms. A vestige of that is the shoulder showing up at high collision energy near the top of the probability curve. Another important difference is the effectiveness of vibrational excitation in enhancing reactivity. In fact, for the 4C processes, the lowering of the threshold in the probability-versus-E_{tr} plots at $v_{ab} = 9-12$ is smaller than that for CID processes. Moreover, threshold values of total energy coincide (as they do for the full-dimensional quantum results at $v_{ab} = 10$, 11[48]). In contrast, when the vibrational excitation is higher ($v_{ab} = 13$, 14) the threshold in total energy is smaller (although still higher than related CID thresholds) due to the higher effectiveness of the vibrational excitation. In any case, however, vibration is always more effective than translation in promoting the exchange reaction.

The SE probabilities are shown in the lower panels of Figure 1. As apparent from the Figure, the threshold values in translational energy decrease with the vibrational excitation. This means that for moderate vibrational excitation ($v_{ab} = 9$, 10, 11), vibrational energy is rather effective (as in the CID and 4C processes), in agreement with the findings of quantum studies.[48] In contrast, at high vibrational excitation, only part of the energy increment is used to lower the threshold of the reactive dissociation processes. Another important difference of SE probabilities from those of CID and 4C processes is their slow increase with translational energy. This makes SE processes unimportant in the considered translational energy interval (except at $v_{ab} = 14$).

QCT versus QM Probabilities

As already mentioned, QCT calculations were performed for a range of initial conditions fully including the QM ones. Thanks to this, it is possible to carry out an extended comparison of our zero total angular momentum QCT results with the QM ones.[48] Both QCT and QM probabilities for $H_aH_b(v_{ab} = 10, 11, j_{ab} = 0) + H_cH_d(v_{cd} = 0, j_{cd} = 0)$ CID, 4C, and SE processes are plotted in Figure 2. As apparent from the Figure, for the CID processes, QCT probabilities well-reproduce the QM ones (including threshold values). However, just past the threshold, the quasiclassical probability becomes slightly larger than the quantum one, but this trend is reverted when energy is further increased. For the 4C processes, QCT and QM results agree even better, with the exception of the threshold region in which QCT values are slightly larger than the QM ones. In contrast, for the SE processes, the QCT probabilities differ (in excess)

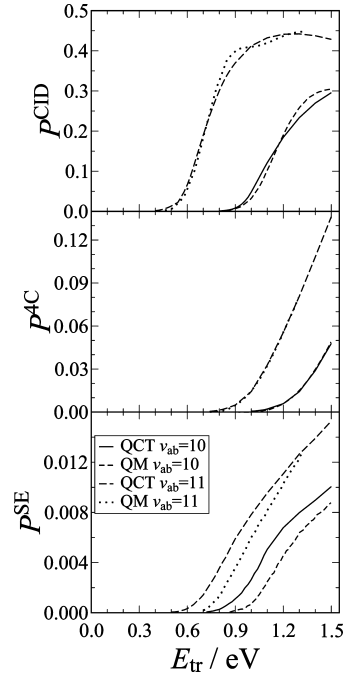

Figure 2. QM and QCT CID (upper panel), 4C (central panel), and SE (lower panel) probabilities calculated at $J = 0$ for H_aH_b ($v_{ab} = 10$, 11, $j_{ab} = 0$) + H_cH_d ($v_{cd} = 0, j_{cd} = 0$) plotted as a function of the collision energy.

significantly from the QM ones, since related thresholds are shifted to lower collision energy. However, it is worth pointing out here that, in this case, the probability values are definitely smaller than those of the other processes, keeping the absolute error small.

To better understand the dynamics of the $H_2 + H_2$ collision can be of help to perform a comparison with reduced dimensionality classical[24] and quantum[23] calculations, yet it is worth noting here that such a comparison can be merely qualitative, since collisions in the H geometry lead only to CID and 4C processes, those in the X and T geometries lead only to CID processes, and those in the L geometries lead only to SE processes. As a matter of fact, the main difference between model and full-dimensional CID probabilities is their absolute value: model probabilities are larger than full-dimensional ones, meaning that constrained geometries are particularly prone to dissociation. Model calculations for the H configuration single out another important feature of the CID probabilities that decrease at the highest energy values of the interval considered, with this decrease not being observed in the results associated with other models and the full-dimensional (both QCT and QM) results.

Full-dimensional QCT and QM CID probability curves exhibit the same threshold values as those obtained in the model classical calculations for H, X, and T geometries. In contrast, the threshold values given by the model quantum calculations are 0.1 eV lower. This difference was attributed by the authors of ref 24 to the fact that the quantum wave packet extends beyond the classical point of return (enhancing accordingly the breaking of the bond due to the rigidity of the model). This rationalizes also the steeper increase in the classical probability curve with respect to the quantum one. A similar feature is found when comparing full-dimensional QCT results with respect to the QM ones. By analogy, this has been attributed to the different abilities of trajectories and wave packets to explore the regions of the potential leading to dissociation after surmounting the barrier.

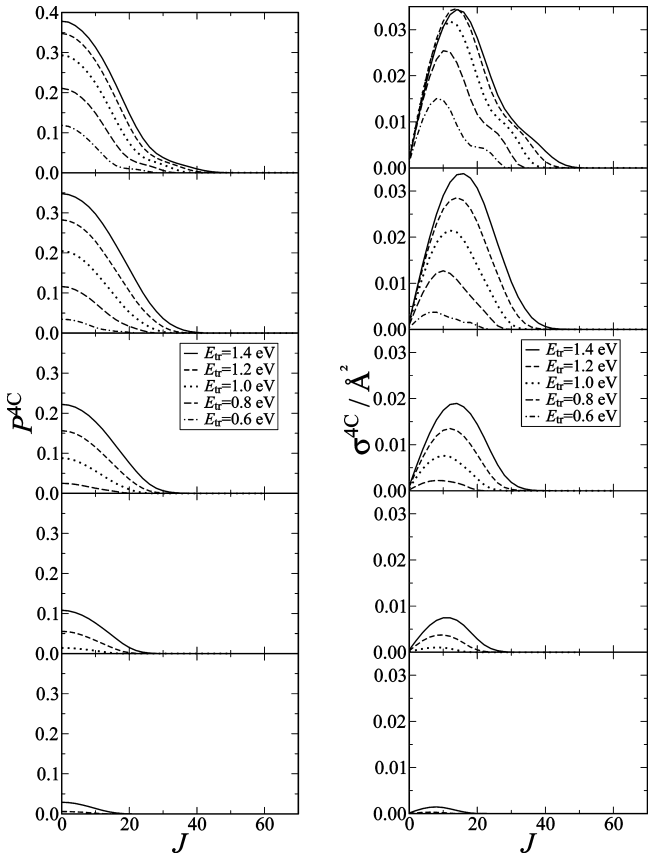

Figure 3. QCT 4C probabilities (left-hand panels) and partial cross sections (right-hand panels) calculated for the collisions H_aH_b (v_{ab}, $j_{ab} = 0$) + H_cH_d ($v_{cd} = 0$, $j_{cd} = 0$) with $v_{ab} = 10$, 11, 12, 13, and 14 (from low panel up) plotted as a function of the total angular momentum quantum number, J.

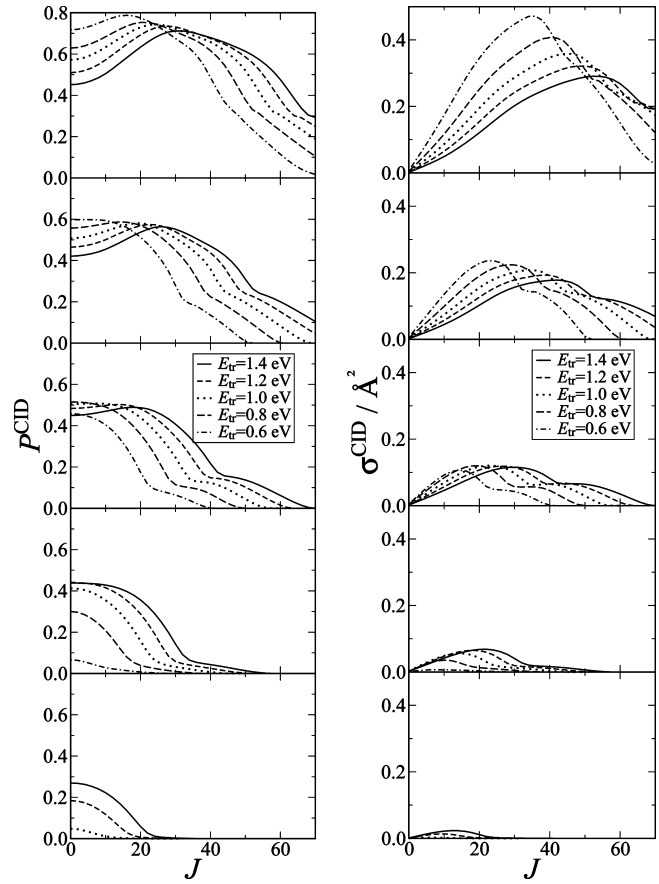

Figure 4. QCT CID probabilities (left-hand panels) and partial cross sections (right-hand panels) calculated for the collisions H_aH_b (v_{ab}, $j_{ab} = 0$) + H_cH_d ($v_{cd} = 0$, $j_{cd} = 0$) with $v_{ab} = 10$, 11, 12, 13, and 14 (from low panel up) plotted as a function of the total angular momentum quantum number, J.

As to the 4C processes, the quantum model (please bear in mind that only the H model geometry allows exchange) exhibits thresholds 0.2 eV lower than those calculated classically, despite the fact that full-dimensional classical and quantum values coincide. Again, this can be attributed to the rigidity of the model, which allows only a partial exploration of the phase space.

Model SE probabilities are significantly larger than full-dimensional ones. Moreover, full-dimensional probabilities show a slow monotonic increase with energy, whereas model ones both increase and decrease quite sharply.

All these differences confirm that model treatments explore a quite biased subset of the reactive dissociative processes and can be used only for qualitative and illustrative purposes.

$J > 0$ Probabilities and Cross Sections

Building on the (just shown) accuracy of the QCT calculations, we used them to carry out an analysis of the effect of increasing J on the efficiency of 4C, CID, and SE processes. Related probabilities (left-hand side panels) and cross sections (right-hand side panels) calculated at different collision energies and initial vibrational states are plotted in Figures 3, 4, and 5 as a function of J.

The first feature of the results worth pointing out here is the increase in the value of J_{max} for all types of processes with both collision and vibrational energy. However, as apparent from Figures 3, 4, and 5, the increase in J_{max} with vibrational energy (from the bottom panels up) is larger than that with collision energy (from internal to external curves within the same panel). This agrees with the consideration that the size of the collision sphere (in a hard sphere model approach) can be straightforwardly related to the vibrational elongation (although this is not so for the collision energy) and varies with the type of process considered. In particular, 4C processes exploit a narrow window of J values that in a hard sphere model approach can be reconducted to a locking radius, depending on the bond length at which the exchange occurs. In contrast, CID can take place at much higher values of the total angular momentum (for example, $J_{max} \approx 120$ when $v_{ab} = 14$ and $E_{tr} = 1.4$ eV) that in the same type of approach (the hard sphere model) can be associated with the radius of optimum vibration−translation energy exchange (that, due to the nature of energy exchanges, is of a less hard type). The difference between 4C and CID processes is further evidenced by the fact that 4C (see left-hand side (lhs) panels of Figure 3) opacity functions (the probability versus J plots of the lhs panels) have a maximum at $J = 0$ and constantly decrease as J increases. In contrast, CID opacity functions (see lhs panels of Figure 4), although having larger absolute values (energy exchange is less selective than mass exchange) and a similar maximum at $J = 0$ for low v_{ab} values, show additional specific features. The first of them is that an increase in v_{ab} eats up the $J = 0$ maximum and leads to a shift of the maximum toward $J = 20-30$ and the formation of either a plateau or a minimum at $J = 0$ that can be understood in terms of a competition by vibrationally induced dissociations.

Another specific feature of the CID opacity functions is the longer tail on the right-hand side (rhs) end of the plots that sometimes grows to form a shoulder. This feature can be

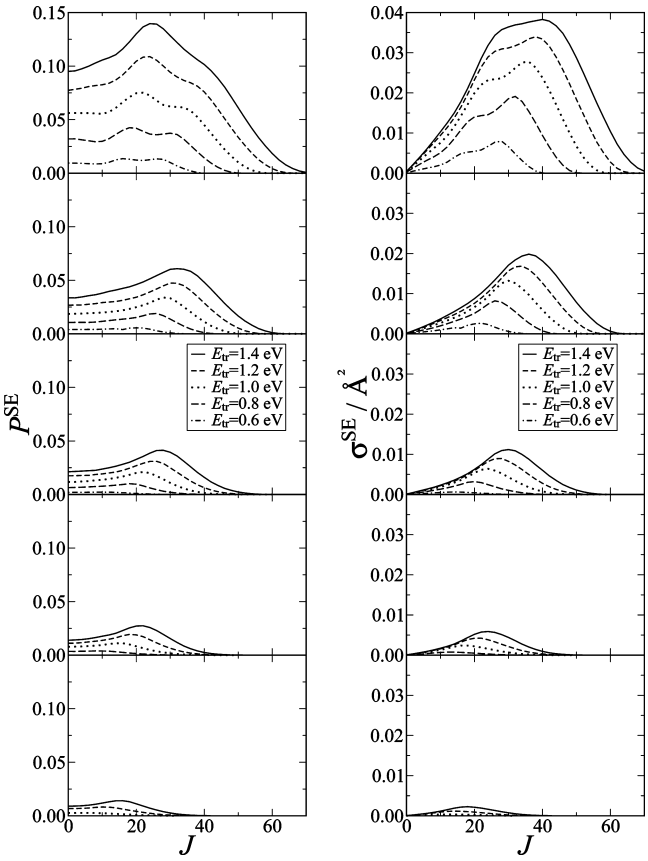

Figure 5. QCT SE probabilities (left-hand panels) and partial cross sections (right-hand panels) calculated for the collisions H_aH_b (v_{ab}, $j_{ab} = 0$) + H_cH_d ($v_{cd} = 0$, $j_{cd} = 0$) with $v_{ab} = 10$, 11, 12, 13, and 14 (from low panel up) plotted as a function of the total angular momentum quantum number, J.

rationalized again in terms of the effect of an increase in J on the dissociation mechanism. The most likely of these events is the dissociation taking place on the side of the impinging H_cH_d molecule to fragment the H_aH_b. Obviously, dissociation can also occur on the opposite side (after a partial orbiting), and this is favored by an increase in J that enhances circumnavigation. Out of the above-mentioned arguments, it is also easy to understand why SE processes, being subject to both exchange and dissociative constraints, are the least likely events and show the $J = 0$ depletion while not exhibiting the high J tail.

In the case of the cross section plotted in the rhs panels of Figures 3, 4, and 5, both the different values of J_{max} for the various processes and the factor $(2J + 1)$ weighing the terms of the sum (see eqs 5 and 6) of the partial probability terms (the partial cross sections) significantly affect the result. As apparent from the plots, high J terms ends up being larger than the low J ones and radically change the slope of the partial (fixed J) cross section curves with respect to the corresponding probability curves. In fact, for example, in the case of 4C reactivity (see Figure 3) the $J = 0$ contribution is completely dominated by larger J terms, giving rise to a maximum located at J values ranging from 4 to 14 in the considered range of translational energy and reactant vibrational excitation. The 4C partial cross section plots also show an extreme case of shift of the maximum along J due to the $(2J + 1)$ factor. This is clearly shown in the right-hand side panels of Figure 3, in which in some cases the tail side of the plots shows even an additional shoulder at high J values. A similar effect also occurs for CID processes (see Figure 4), for which both the depressing effect at $J = 0$ and the enhancement of the higher J region (including the shoulder) are quite pronounced. In this case, in fact, the higher J structure shows up at all v_{ab} values larger than 10. The effect of J on the SE partial cross section (see Figure 5) is also quite evident. In fact, not only is the $J = 0$ suppression even enhanced due to the fact that the probability itself is small at zero total angular momentum, but also the higher J shoulder becomes in some cases a new (larger) maximum.

From partial cross sections, one can evaluate integral cross sections using eq 6. Calculated values substantially confirm the estimates obtained by sampling randomly the values of the total angular momentum,[32] which increase regularly with vibrational and collisional energy (with the exception of CID for $v_{ab} = 14$). The key point to emphasize here is the fact that, contrary to what is found for the $J = 0$ contributions, CID cross sections are more than 1 order of magnitude larger than those of SE and 4C processes, as expected from the different values of J_{max}.

The above discussion leads naturally into the question of to what extent the $J = 0$ full-dimensional quantum calculations of ref 48 can be used (once properly shifted along the collision energy) to represent the higher J reactivity of the $H_2 + H_2$ system. The answer to this question is of paramount importance to establish the validity of J-shift model approaches to reactivity.[56] In the J-shift model treatment, in fact, higher J probabilities are approximated by the $J = 0$ ones after shifting them in energy by the amount associated with the overall rotation of the system computed for its saddle rigid collinear tetraatomic geometry. To discuss the validity of the J-shift model, related probabilities obtained from $J = 0$ 4C probabilities are compared with the calculated $J > 0$ QCT probabilities (see Figure 6). As apparent from the figure, results obtained from the J-shift model well reproduce the $J > 0$ probabilities at low J values, whereas at high J values, they underestimate them, indicating that the shift in energy with J is too large or that the effect of increasing J on the state to the probability is insufficiently rendered by a shift in energy. Significant effects, though opposite in sign, also show up at high vibrational excitation and large collision energy for which the shift in energy results to be too small, since the J-shift probabilities overestimate the one calculated at fixed lower J values, and as J increases, they steeply decrease, vanishing at small value of J_{max}. In all cases, however, J-shift results miss the high J tail that turns out to be the most important contribution to the evaluation of the cross section and, as a consequence, of the rate coefficients that play a crucial role in determining the kinetics of nonequilibrium chemical systems.

Product Vibrational and Rotational Distributions

Of key importance for the modeling of complex chemical systems under nonequilibrium thermal conditions (such as plasmas or interstellar clouds under shock waves) are also the values of the state-to-state properties, which have recently become the object of intense investigation.[57] For this reason, we devote the last part of this paper to the analysis of product vibrational and rotational distributions.

In the H_aH_b (v_{ab} = high, $j_{ab} = 0$) + H_cH_D ($v_{cd} = 0$, $j_{cd} = 0$) CID processes, collisions almost exclusively lead to the breaking of the highly excited molecule, with only a negligible fraction of 0.2% of the molecules initially in the ground state dissociating. The nondissociated molecules remain mainly in the ground vibrational state with at most (for $J = 0$, $v_{ab} = 14$ and $E_{tr} = 1.4$ eV) a mere 2% being promoted to the $v'_{cd} = 1$ excited state and a truly negligible fraction populating $v'_{cd} = 2$. In addition, the rotational excitation is scarce. In fact, the final rotational quantum number hardly reaches the value $j'_{cd} = 5$ and is even lower at higher J.

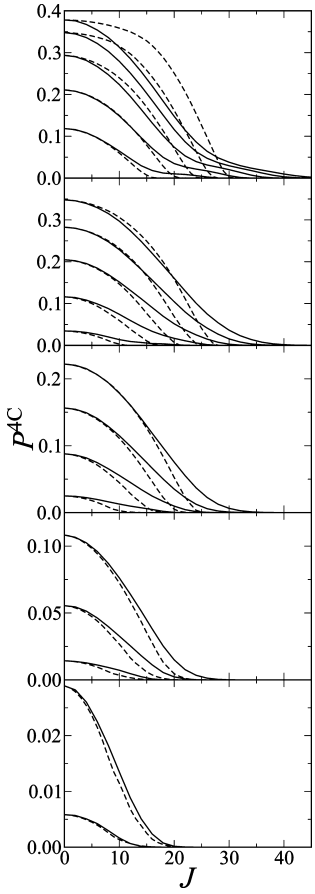

Figure 6. QCT (solid lines) and *J*-shift (dashed lines) 4C probabilities calculated for the collisions H_aH_b (v_{ab}, $j_{ab} = 0$) + H_cH_d ($v_{cd} = 0$, $j_{cd} = 0$) with $v_{ab} = 10$, 11, 12, 13, and 14 (from low panel up) plotted as a function of the total angular momentum, *J*. Within the same panel, collision energy (1.4, 1.2, 1.0, 0.8, 0.6 eV) decreases from external to internal curves. Scales have been modified with respect to Figure 3.

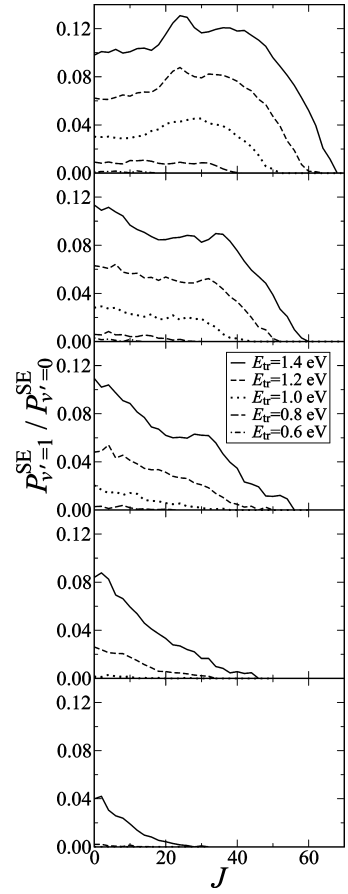

Figure 7. QCT $P^J_{v'=1}/P^J_{v'=0}$ ratio for the SE processes calculated for the collisions H_aH_b (v_{ab}, $j_{ab} = 0$) + H_cH_d ($v_{cd} = 0$, $j_{cd} = 0$) with $v_{ab} = 10$, 11, 12, 13, and 14 (from low panel up) plotted as a function of the total angular momentum quantum number, *J*.

SE processes produce only one hydrogen molecule formed by atoms of different initial molecules with probability significantly lower than that of the CID processes. However, contrary to the CID case, molecules produced by the SE processes can be vibrationally excited. As a matter of fact, the probability for populating the first excited vibrational state is more than 5 times larger than that of the CID collisions (the population of the state $v' = 2$ is less than 0.7%). Figure 7 shows the ratio between the probability of populating the state $v' = 1$ and that of populating the ground vibrational state $v' = 0$ for several collision energies and different initial vibrational states plotted as a function of the total angular momentum quantum number, *J*. As apparent from the figure, the population of $v' = 1$ can be as high as 0.13 for the highest initial vibrational state and the highest collision energy considered here. When the initial vibrational excitation is low, only collisions with a small total angular momentum appreciably populate the first excited vibrational state of the products. Such a population increases with the initial vibrational and collision energy. At the same time, it decreases almost linearly as *J* increases, with the slope becoming sharper as the collision energy increases. However, when the initial vibrational excitation increases, the interval of values of *J* leading to an appreciable population of product excited molecules widens. This feature is independent of the value of the probability, whose maximum, as already indicated, is not located at $J = 0$. When collisions take place with $v_{ab} = 14$, the interval of values of *J* leading to product excited molecules further widens, and the maxima appear at relatively high total angular momentum values.

SE processes also lead to rotationally excited product molecules. The rotational excitation increases with both vibrational and collision energy. In particular, at $J = 0$, the maximum rotational quantum number goes from $j' = 3$ (and $v' = 0$) for $v_{ab} = 11$ and $E_{tr} = 0.60$ eV to $j' = 11$ (and $v' = 0$) for $v_{ab} = 14$ and $E_{tr} = 1.40$ eV, being the rotational states with maximum population $j' = 1$ and $j' = 3$, respectively. Moreover, the rotational excitation for $v' = 1$ is only slightly smaller than that for $v' = 0$. As the total angular momentum increases, the maximum final rotational quantum number populated is lower by one or two units than that found at $J = 0$, and the rotational quantum state with maximum population can shift up to $j' = 6$.

Product vibrational distributions of exchange reactive processes (4C processes) are obviously much richer due to the formation of two new product hydrogen molecules. For illustrative purposes, Figure 8 shows the contour plots of the correlation probability of populating two given final vibrational states, v'_1 and v'_2, for collisions starting with $v_{ab} = 13$ and $E_{tr} = 1.2$ eV. As apparent from the figure, a dramatic effect is produced by a variation of the total angular momentum quantum number. At $J = 0$, in fact, the product vibrational distribution differs significantly from that of reactants in that it shows (upper left panel of Figure 8) two maxima. The first maximum (that is also the highest) corresponds to a mild vibrational excitation of the two product molecules (in the Figure, $v'_1 = 4$ and $v'_2 = 3$, respectively). The second maximum corresponds, instead, to an

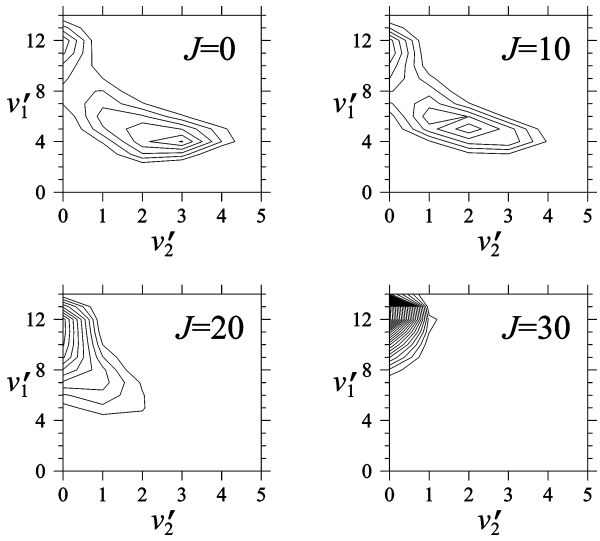

Figure 8. Contour plots (v'_1 vs v'_2) of the relative QCT product vibrational distributions for the 4C processes of the H_aH_b ($v_{ab} = 13, j_{ab} = 0$) + H_cH_d ($v_{cd} = 0, j_{cd} = 0$) collisions at $E_{tr} = 1.2$ eV. Contour lines differ by 0.01.

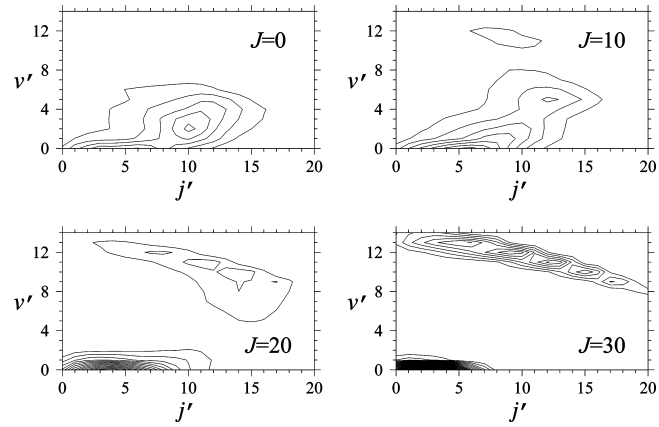

Figure 9. Contour plots (v' vs j') of the relative QCT product vibrational and rotational distribution for the 4C processes of the H_aH_b ($v_{ab} = 13, j_{ab} = 0$) + H_cH_d ($v_{cd} = 0, j_{cd} = 0$) collisions at $E_{tr} = 1.2$ eV. Contour lines differ by 0.003.

almost adiabatic vibrational distribution mimicking that of the initial vibrational states: one of the formed molecules is highly vibrationally excited, with a vibrational quantum number equal to or slightly lower than v_{ab}, whereas the other is in its ground or first excited vibrational state, such as v_{cd}. As the total angular momentum increases, the first maximum tends to vanish in favor of a more pronounced difference between the two product vibrational states. For example, Figure 8 shows that at $J = 10$, this maximum occurs when both product molecules populate $v'_1 = 5$ and $v'_2 = 2$ with a probability about equal to that of the second maximum. At high values of J, the first maximum disappears (in the figure, this occurs for $J \geq 20$). Accordingly, one of the two new molecules has null or scarce excitation, and the other one has a vibrational excitation similar to v_{ab}, despite the fact that vibrational de-excitation can still be important (for example, a nonnegligible population of the vibrational state with a quantum number of 6 at $J = 24$).

Both the initial vibrational excitation and the collision energy play a significant role in the product vibrational distribution. In fact, high values of v_{ab} tend to favor the production of molecules with low vibrational excitation, despite the large jump in vibrational excitation. This is more important at low collision energies when collisions with high values of v_{ab} lead only to the first maximum and collisions with low values of v_{ab} lead only to the second maximum. Collision energy also has an important effect on the value of the total angular momentum at which the first maximum disappears. As the collision energy decreases, in fact, the value of the total angular momentum quantum number for which the second maximum disappears decreases. For example, at $v_{ab} = 13$ and $E_{tr} = 0.6$, 0.8, 1.0, and 1.2 eV, the vanishing of the first maximum occurs starting from $J = 12$, 18, 20, and 22, respectively.

For 4C processes, it is also interesting to analyze the rotational distribution of the product molecules. It does, in fact, differ from that of the dissociation processes, since formed product molecules can be highly rotationally excited. For illustrative purposes, Figure 9 shows the contour plots for the correlation probability of populating a given vibrational state, v', and a given rotational state, j', of the formed molecules corresponding to the same 4C processes considered in Figure 8. As apparent from the figure, at $J = 0$, the molecules formed in the lowest vibrational states can be rotationally excited up to $j' = 15$ with a maximum at $v' = 2$ and $j' = 10$. Little rotational excitation is instead obtained for highly excited vibrational products. The same behavior is observed up to $J = 10$ whereas for $J \geq 20$, the behavior is of the opposite nature. This means that a limited rotational excitation is observed when products are vibrationally cold ($v' \leq 2$) but strong excitation to the limit value for the dissociation is observed for highly vibrationally products.

Conclusions

The calculation of the various processes taking place when two hydrogen molecules collide has been investigated in detail by carrying out extended computational campaigns on the segment of the European Computing Grid available to the virtual organization COMPCHEM and on the Spanish Supercomputing Network. The positive impact of using concurrent platforms is apparent from the high numerical precision of the calculated state-specific and state-to-state probabilities. Thanks to this, some peculiar structures and a fingerprint of different collisional mechanisms occurring even for the same type of process (say, dissociative collisions, for example) have been evidenced. Other important features of the investigated processes singled out by the extended computational campaigns are (1) the impressive ability of quasiclassical trajectory outcomes to reproduce quantum results; (2) the dominance of CID processes due to the scarce selectivity of vibrational−translational energy exchange; (3) the higher efficiency of vibration (rather than translation) in promoting dissociation and reaction; (4) the strong bias of reduced dimensionality models toward some specific outcomes of the collisional process; (5) the possibility of evidencing the limits of the J-shift model when calculating higher J probabilities and cross sections; (6) the thinness of the J values interval, leading to exchange compared with the wideness of that associated with dissociative processes; (7) the dependence on J of some collision mechanisms and of the different efficiencies of the various collision parameters; and (8) the ability of internal energy product distributions to reflect the particular dynamics of some processes, such as the significant vibrational excitation associated with SE processes and the large vibrational deactivation associated with the 4C ones as compared with the substantial vibrational adiabaticity of CID processes.

Acknowledgment. Partial financial support from MICINN (CTQ-2008-02578/BQU), MIUR, EGEE III, and ARPA Umbria

is acknowledged. This work has been carried out also as part of the activities of the cooperation scheme of the QDYN working group of the COST CMST European Cooperative Project CHEMGRID (Action D37). Computational assistance and resources were provided also by the SGI/IZO-SGIker at the UPV/EHU and by the Spanish Supercomputing Network (RES).

References and Notes

(1) Schwenke, D. W. *J. Chem. Phys.* **1988**, *89*, 2076.
(2) Schwenke, D. W. *J. Chem. Phys.* **1990**, *92*, 7267.
(3) Capitelli, M., Barsdley, J. N. Eds.; *Non-equilibrium processes in partially ionized gases*; Plenum: New York, 1990.
(4) Park, C. *Int. J. Thermophys.* **1993**, *7*, 385.
(5) Capitelli, M.; Celiberto, R.; Esposito, F.; Laricchiuta, A.; Hassouni, K.; Longo, S. *Plasma Sources Sci. Technol.* **2002**, *11*, A7.
(6) Diomede, P.; Longo, S.; Capitelli, M. *Eur. Phys. J. D* **2005**, *33*, 243.
(7) Capitelli, M.; Cacciatore, M.; Celiberto, R.; De Pascale, O.; Diomede, P.; Esposito, F.; Gicquel, A.; Gorse, C.; Hassouni, K.; Laricchiuta, A.; Longo, S.; Pagano, D.; Rutigliano, M. *Nucl. Fusion* **2006**, *46*, S260.
(8) Draine, B. T. *Astrophys. J.* **1980**, *241*, 1021.
(9) Shull, J. M.; Draine, B. T. In *Interstellar processes*; Hollenbach, D. J., Thronson, H. A., Eds.; Reidel: Dordrecht, 1987, p 283.
(10) Hollenbach, D. J.; McKee, C. F. *Astrophys. J.* **1989**, *342*, 306.
(11) Dove, J. E.; Rusk, A. C. M.; Kribb, P. H.; Martin, P. G. *Astrophys. J.* **1987**, *318*, 379.
(12) Martin, P. G.; Keogh, W. J.; Mandy, M. E. *Astrophys. J.* **1998**, *499*, 793.
(13) Siegban, P.; Liu, B. *J. Chem. Phys.* **1978**, *68*, 2457.
(14) Boothroyd, A. I.; Dove, J. E.; Keogh, W. J.; Martin, P. G.; Peterson, M. R. *J. Chem. Phys.* **1991**, *95*, 4331.
(15) Boothroyd, A. I.; Martin, P. G.; Keogh, W. J.; Peterson, M. R. *J. Chem. Phys.* **2002**, *116*, 666.
(16) Aguado, A.; Suárez, C.; Paniagua, M. *J. Chem. Phys.* **1994**, *101*, 4004.
(17) Garcia, E.; Laganà, A. *Mol. Phys.* **1985**, *56*, 621.
(18) Garcia, E.; Laganà, A. *Mol. Phys.* **1985**, *56*, 629.
(19) Truhlar, D. G.; Horowitz, C. J. *J. Chem. Phys.* **1978**, *68*, 2466.
(20) Hernández, M. I.; Clary, D. C. *J. Chem. Phys.* **1996**, *104*, 8413.
(21) Di Domenico, D.; Hernández, M. I.; Campos-Martínez, J. *J. Chem. Phys.* **2001**, *342*, 177.
(22) Hernández, M. I.; Campos-Martínez, J.; Van Caillie, C.; Di Domenico, D. *Mol. Phys.* **2004**, *102*, 2335.
(23) Bartolomei, M.; Hernández, M. I.; Campos-Martínez, J. *J. Chem. Phys.* **2005**, *122*, 0643055.
(24) Carmona-Novillo, E.; Bartolomei, M.; Hernández, M. I.; Campos-Martínez, J. *J. Chem. Phys.* **2007**, *126*, 124315.
(25) Bauer, S. H.; Resker, E. E. L. *Science.* **1964**, *146*, 1045.
(26) Silver, D. M.; Stevens, M. R. *J. Chem. Phys.* **1973**, *59*, 3378.
(27) Brown, N. J.; Silver, D. M. *J. Chem. Phys.* **1976**, *65*, 31178.
(28) Brown, N. J.; Silver, D. M. *J. Chem. Phys.* **1980**, *72*, 3869.
(29) Raz, T.; Levine, R. D. *Chem. Phys. Lett.* **1994**, *226*, 47.
(30) Raz, T.; Levine, R. D. *J. Phys. Chem.* **1995**, *99*, 7435.
(31) Raz, T.; Levine, R. D. *J. Phys. Chem.* **1995**, *99*, 13713.
(32) Ceballos, A.; Garcia, E.; Rodríguez, A.; Laganà, A. *Chem. Phys. Lett.* **1999**, *305*, 276.
(33) Ceballos, A.; Garcia, E.; Rodríguez, A.; Laganà, A. *J. Phys. Chem. A* **2001**, *105*, 1797.
(34) Ceballos, A.; Garcia, E.; Rodríguez, A.; Laganà, A. *Phys. Chem. Chem. Phys.* **2002**, *4*, 5007.
(35) Ceballos, A.; Garcia, E.; Laganà, A. *J. Phys. Chem. Ref. Data* **2002**, *31*, 371.
(36) Mandy, M. E.; Martin, P. G.; Keogh, W. J. *J. Chem. Phys.* **1998**, *108*, 492.
(37) Mandy, M. E.; Rothwell, T. A.; Martin, P. G. *J. Chem. Phys.* **2001**, *114*, 10780.
(38) Pogrebnya, S. K.; Clary, D. C. *Chem. Phys. Lett.* **2002**, *363*, 523.
(39) Pogrebnya, S. K.; Mandy, M. E.; Clary, D. C. *Int. J. Mass Spectrom.* **2003**, *223*−*224*, 335.
(40) Mandy, M. E.; Pogrebnya, S. K. *J. Chem. Phys.* **2004**, *120*, 5585.
(41) Quéméner, G.; Balakrishnan, N.; Krems, R. V. *Phys. Rev. A* **2008**, *77*, 030704(R).
(42) Quéméner, G.; Balakrishnan, N. *J. Chem. Phys.* **2009**, *130*, 114303.
(43) Lin, S. Y.; Guo, H. *J. Chem. Phys.* **2002**, *117*, 5183.
(44) Lin, S. Y.; Guo, H. *Chem. Phys.* **2003**, *289*, 191.
(45) Gatti, F.; Otto, F.; Sukiasyan, S.; Meyer, H.-D. *J. Chem. Phys.* **2005**, *123*, 174311.
(46) Panda, A. N.; Otto, F.; Gatti, F.; Meyer, H.-D. *J. Chem. Phys.* **2007**, *127*, 174310.
(47) Otto, F.; Gatti, F.; Meyer, H.-D. *J. Chem. Phys.* **2008**, *128*, 064305.
(48) Lu, Y.; Lee, S. Y.; Zhang, D. H. *J. Chem. Phys.* **2006**, *124*, 011101.
(49) Lu, Y.; Zhang, D. H.; Lee, S. Y. *Chem. Phys.* **2005**, *308*, 217.
(50) Hase, W. L.; Duchovic, R. J.; Hu, X.; Komornicki, A.; Lim, K. F.; Lu, D.; Peslherbe, G. H.; Swamy, K. N.; Van de Linde, S. R.; Varandas, A. J. C.; Wang, H.; Wolf, R. J. *VENUS96: A General Chemical Dynamics Program*; QCPE Program N. 671, Indiana University: Bloomington, IN, 1996.
(51) Aoiz, F. J.; Sáenz-Rábanos, V.; Martínez-Haya, B.; González-Lezana, T. *J. Chem. Phys.* **2005**, *123*, 094110.
(52) http://www.bsc.es; Barcelona Supercomputing Centre − Red Española de Supercomputación. (Accessed June 10, 2009.)
(53) http://www.eu-egee.org; Enabling Grids for E-Science in Europe (EGEE). (Accessed June 10, 2009.)
(54) http://www.compchem.unipg.it; COMPCHEM Virtual Organization. (Accessed June 10, 2009.)
(55) Laganà, A.; Riganelli, A.; Gervasi, O. *Lect. Notes Comput. Sci.* **2006**, *665*, 3980.
(56) Bowman, J. M. *J. Phys. Chem.* **1991**, *95*, 4960.
(57) Casavecchia, P. *Rep. Prog. Phys.* **2000**, *63*, 355.

JP903072J